Mechanics of Materials 160 (2021) 103959

Contents lists available at ScienceDirect

Mechanics of Materials

journal homepage: www.elsevier.com/locate/mechmat

Stress relaxation in high-entropy $Pd_{20}Pt_{20}Cu_{20}Ni_{20}P_{20}$ metallic glass: Experiments, modeling and theory

Y.J. Duan [a,b], J.C. Qiao [a,*], T. Wada [c], H. Kato [c], E. Pineda [b], D. Crespo [b], Yun-Jiang Wang [d,e,**]

[a] School of Mechanics, Civil Engineering and Architecture, Northwestern Polytechnical University, Xi'an, 710072, China
[b] Department of Physics, Institute of Energy Technologies, Universitat Politècnica de Catalunya, Barcelona, 08019, Spain
[c] Institute for Materials Research, Tohoku University, Sendai, 980-8577, Japan
[d] State Key Laboratory of Nonlinear Mechanics, Institute of Mechanics, Chinese Academy of Sciences, Beijing, 100190, China
[e] School of Engineering Science, University of Chinese Academy of Sciences, Beijing, 101408, China

ARTICLE INFO

Keywords:
High-entropy metallic glass
Stress relaxation
Linear relaxation model
Structural heterogeneity
Viscoelastic deformation

ABSTRACT

The viscoelastic properties of $Pd_{20}Pt_{20}Cu_{20}Ni_{20}P_{20}$ high-entropy metallic glass were probed by dynamic mechanical spectroscopy and stress relaxation. The experimental evolution of stress can be characterized by the empirical Kohlrausch-Williams-Watts function during the tensile stress relaxation measurement. We develop a linear relaxation model able to describe the whole process of stress relaxation in a wide range of temperatures. The linear relaxation model takes into account the microstructural heterogeneity of the glass, and thus its dynamical heterogeneity, so that the thermal effect and stress-driven process are physically decoupled. The activation energy spectra at various temperatures reveal the changes of the deformation units during stress relaxation, which is the result of the interplay between stress and temperature. This study decomposes the widespread hierarchical dynamics due to structural heterogeneity which accommodates the viscoelastic deformation of the high-entropy metallic glasses.

1. Introduction

Metallic glasses (MGs) have attracted large interest during the last decades, because they exhibit promising mechanical, chemical and physical properties (Fornell et al., 2009; Hufnagel et al., 2016; Inoue and Takeuchi, 2011; Johnson, 1999; Kato et al., 2006; Schroers and Johnson, 2005; Schuh et al., 2007; Sun and Wang, 2015; Wang, 2012; Wang et al., 2018b). However, due to their disordered structure, it is still very challenging to correlate the mechanical/physical properties with the structural and microstructural features of MGs (Cheng and Johnson, 1987; Greer, 1993; Highmore and Greer, 1989; Launey et al., 2009; Spaepen, 1987; Wang, 2011).

Compared with crystalline alloys, MGs lack long-range periodic arrangement of atoms. However, they show short- and medium-range order, revealed by both computer simulations and experimental structural characterization (Cheng and Ma, 2011; Hirata et al., 2011; Sheng et al., 2006). Conventional characterization techniques show that MGs have an amorphous structure at the atomic level, subnanometer scale, and they were considered as "homogeneous" at early stage (Masumoto and Hashimoto, 1978). However, later literature proved that the atomic structure of MGs contains local structural heterogeneity, which is closely linked to the local static and dynamic properties (Fujita et al., 2009; Kim et al., 2013; Kim et al., 2006; Y. C. Hu et al., 2016; Zhu et al., 2017). Nowadays, it is believed that structural heterogeneity plays a central role in understanding the physical and mechanical behaviors of MGs (Tsai et al., 2017; Zhu et al., 2016).

Structural heterogeneity of MGs has been observed at different length scales both experimentally (Ichitsubo et al., 2005; Wang et al., 2014b) and in atomistic simulations (Cheng and Ma, 2011; Fujita et al., 2009). Numerous studies attempted to reveal the intrinsic correlation between structural heterogeneity and mechanical/physical properties of MGs, such as the elastic constants (Flores et al., 2007; Ngai et al., 2014), ductility (Bharathula and Flores, 2011), cryogenic thermal cycling effects (Ketov et al., 2015; Vempati et al., 2012), liquid-liquid phase separation (Tanaka, 2012; Wang, 2012), and nano-glass structure (García et al., 2007; Gleiter, 2016; Sha et al., 2017; Wang et al., 2014a). Nevertheless, despite early and recent research efforts, it is still difficult to elucidate the connection between structural heterogeneity and

* Corresponding author.
** Corresponding author.
E-mail addresses: qjczy@nwpu.edu.cn (J.C. Qiao), yjwang@imech.ac.cn (Y.-J. Wang).

https://doi.org/10.1016/j.mechmat.2021.103959
Received 9 December 2020; Received in revised form 5 June 2021; Accepted 15 June 2021
Available online 21 June 2021

macroscopic mechanical behavior.

MGs based on a majority element (i.e. Cu, Zr, Ti, Mg) show a limited glass-forming ability (GFA) (Inoue and Takeuchi, 2011). More recently, high-entropy alloys (HEAs) containing five or more main elements with near-equal or equal atomic contents have been developed (Glasscott et al., 2019; Goncharova et al., 2017; Wang, 2014). Owing to the equimolar concentrations of each element, high-entropy crystalline alloys usually possess distinctive mechanical and physical properties, e.g. high configurational-entropy, sluggish diffusion and severe lattice distortion as well as the cocktail effect (George et al., 2019; Miracle and Senkov, 2017; Zhang et al., 2021a). Inheriting some properties of both MGs and HEAs, high-entropy metallic glasses (HE-MGs) sometimes exhibit superior mechanical properties, i.e. ultrahigh strength at ambient temperature (Kim et al., 2018), excellent wear resistance (Shu et al., 2017) and a sluggish diffusion (Yang et al., 2016; Zhang et al., 2016). As a consequence, HE-MGs open a new avenue in potential applications as both functional and structural materials (Cunliffe et al., 2012). Moreover, the concept of high entropy may provide plenty of new compositional and structural configurations that can facilitate constructing a correlation between mechanical properties and microscopic structure.

The $Pd_{20}Pt_{20}Cu_{20}Ni_{20}P_{20}$ HE-MG is related to $Pd_{40}Ni_{40}P_{20}$, a prototypical MG which has been widely studied in many aspects: the evolution of shear bands at different strains and strain rates (Xu and Shi, 2018), the atomic diffusivity and viscosity near the glass transition temperature (Duine et al., 1993) and the formation volume of defects with pressure-induced structural relaxation (Ruitenberg et al., 1997). The $Pd_{20}Pt_{20}Cu_{20}Ni_{20}P_{20}$ HE-MG has a large glass forming ability (GFA), being possible to cast parts with more than 10 mm of diameter and fully amorphous structure (Takeuchi et al., 2011). Benefitting from a wide supercooled liquid temperature range of 65 K and a reduced glass transition temperature of 0.71 (Takeuchi et al., 2011), the $Pd_{20}Pt_{20}Cu_{20}Ni_{20}P_{20}$ glassy system is a potential model alloy to study the physical and mechanical properties of high-entropy metallic glasses.

The mechanical evolution of MGs has been intensely explored by dynamic mechanical analysis (DMA) (Jeong et al., 2004; Ju and Atzmon, 2014), creep (Bobrov et al., 2007; Herrero-Gómez and Samwer, 2016; Komazaki et al., 2009; Krisponeit et al., 2014; Li et al., 2019; Lu et al., 2014; Qiao et al., 2019a; Wang et al., 2018a) and stress relaxation (Lei et al., 2020; Qiao et al., 2015, 2016; Wang et al., 2014b). Stress relaxation, in particular, has proven to be a powerful tool in the characterization of dynamic heterogeneities as well as the distribution of structural heterogeneity (i.e. deformation units) in MGs (Jiao et al., 2013a; Wang et al., 2014b; Zhao et al., 2015). Since the $Pd_{20}Pt_{20}Cu_{20}Ni_{20}P_{20}$ HE-MG was derived from the ternary $Pd_{40}Ni_{40}P_{20}$ bulk metallic glass by Takeuchi in 2011 (Takeuchi et al., 2011), the characterization of its structural heterogeneity and possible relationship with its mechanical properties has not only intrinsic interest but it can also reveal some clues that can derive from the comparison with its parent alloy.

The aim of the current work is to probe the structural heterogeneity of the high-entropy $Pd_{20}Pt_{20}Cu_{20}Ni_{20}P_{20}$ MG by performing stress relaxation experiments in a wide temperature window. The stress relaxation spectrum is described by the Kohlrausch-Williams-Watts (KWW) function. In parallel, a linear relaxation model of stress relaxation, considering the microstructural heterogeneity, is proposed to describe the stress relaxation behavior. Subsequently, we compute the activation energy spectra at various temperatures in order to physically decouple the hierarchical viscoelastic mechanisms. Finally, the computed and experimental stress relaxation results over a wide range of temperatures are discussed in terms of the distribution of thermally activated mechanisms.

2. Materials and experimental procedure

2.1. Sample fabrication

Due to its excellent GFA and high thermal stability (Takeuchi et al., 2011), $Pd_{20}Pt_{20}Cu_{20}Ni_{20}P_{20}$ HE-MG was selected as a model alloy. The master alloy was prepared by the B_2O_3 flux method (Takeuchi et al., 2011). Metal chips of Pd (99.9%), Pt (99.9%), Cu (99.9%), Ni (99.9%) and lumps of P (99.9%) were mixed together in a sealed and evacuated quartz tube, the ingot was re-melted several times to ensure chemical homogeneity under inert argon in a resistance heating furnace. Bulk samples were produced by copper casting, while ribbon samples were fabricated by the melt spinning technique, with a cross section of 0.02 mm $\times$ 1.2 mm.

2.2. X-ray diffraction (XRD)

X-ray diffraction (XRD) was performed at room temperature to characterize the amorphous nature of $Pd_{20}Pt_{20}Cu_{20}Ni_{20}P_{20}$ HE-MG by Cu Kα radiation in a commercial device (D8, Bruker AXS Gmbh).

2.3. Differential scanning calorimetry (DSC)

The thermal properties (i.e. the glass transition temperature T_g and the onset crystallization temperature T_x) of the $Pd_{20}Pt_{20}Cu_{20}Ni_{20}P_{20}$ HE-MG were determined by differential scanning calorimetry (DSC, Netzsch 202) in high purity dry nitrogen atmosphere at a heating rate of 10 K/min. Aluminum pans were used as sample holders. Baseline correction during the experiment was made for the DSC curve. The temperature was calibrated prior to the experiments with Indium and Zinc standard specimens.

2.4. Mechanical spectroscopy

Dynamic mechanical analysis (DMA, TA instruments Q800) is an effective method to probe the mechanical response of glassy materials. Here we performed DMA on ribbon and bulk specimens. Experimental bulk specimens with dimensions of 30 mm (length) $\times$ 2 mm (width) $\times$ 1 mm (thickness) were cut by automatic wire cutting machines. The surface of the specimens was polished using diamond paste. In the DMA experiment, a periodic stress was applied, and the corresponding strain was recorded. The complex modulus $E^* = E' + iE''$ was computed, so as the storage modulus E' and loss modulus E'' were determined. The loss factor (also named internal friction) $\tan\delta = \frac{E''}{E'}$ was also obtained. The strain amplitude was lower than 10^{-3}. Ribbon DMA measurements were performed while heating at a constant heating rate at a constant frequency (ranging from 0.5 Hz to 8 Hz). Bulk samples were heated to the desired temperature (425-430-435 … 580 K) and its response in frequency (ranging from 10^{-2} to 16 Hz) was recorded.

2.5. Stress relaxation measurement

Tensile stress relaxation experiments were carried out on ribbon samples on the TA Q800 DMA, in a nitrogen-flushed atmosphere. A step strain of 0.4% was instantaneously applied. After reaching the desired test temperature, the ribbon was equilibrated for 5 min prior to the application of the deformation, and they were allowed to relax for 960 min at constant strain conditions.

3. Results and discussion

3.1. XRD analysis and thermal properties

The XRD pattern of the $Pd_{20}Pt_{20}Cu_{20}Ni_{20}P_{20}$ HE-MG is displayed in Fig. 1 (a), showing a broad diffraction peak and no signs of any crystalline phase. Therefore, the amorphous nature of the HE-MG is verified.

Fig. 1 (b) shows the DSC curve of $Pd_{20}Pt_{20}Cu_{20}Ni_{20}P_{20}$ HE-MG at a heating rate of 10 K/min. The glass transition temperature $T_g = 572$ K and the onset crystallization temperature $T_x = 632$ K are determined. It should be noted that the supercooled liquid region (SLR) $\Delta T = T_x - T_g =$

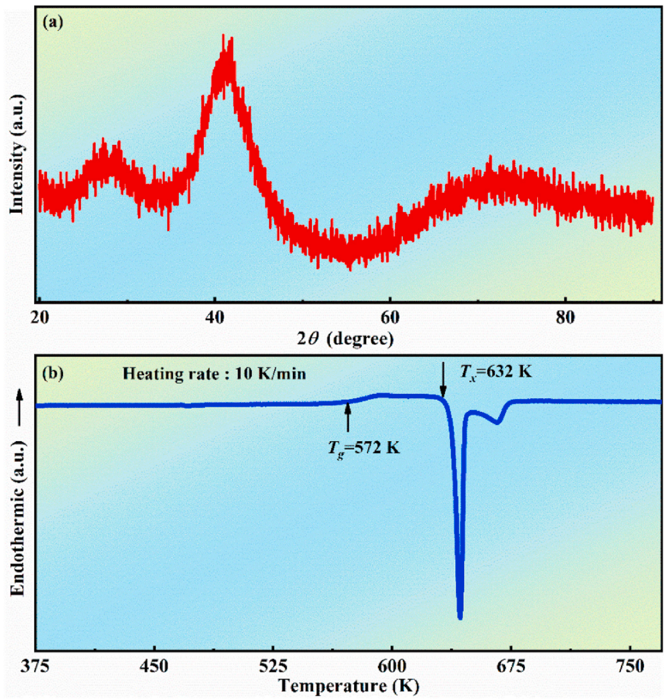

Fig. 1. (a) XRD pattern of the as-cast state. The morphology confirms the amorphous nature of $Pd_{20}Pt_{20}Cu_{20}Ni_{20}P_{20}$. (b) DSC curve at a heating rate of 10 K/min. The glass transition temperature T_g and the onset crystallization temperature T_x are pointed by the arrows in the figure.

60 K is large, which indicates that $Pd_{20}Pt_{20}Cu_{20}Ni_{20}P_{20}$ HE-MG exhibits excellent glass forming ability. Hence, it can be used as an excellent model alloy to study the dynamic mechanical and stress relaxation behaviors.

3.2. Dynamic mechanical analysis

As temperature increases two main mechanical relaxation modes are found in MGs (Harmon et al., 2007), (I) The slow β relaxation (Qiao et al., 2018; Wang et al., 2015), which is a thermodynamically reversible process related to local atomic or molecular rearrangement. Recent investigations showed that the slow β relaxation is linked with the plastic deformation and the nature of the glass transition of MGs (Zhang et al., 2019). Here it should be noted that another process, the fast β relaxation, with shorter characteristic times, would be observed at lower temperatures or higher frequencies. (II) The primary α relaxation, which is linked to a large scale atomic or molecular cooperative movement and the dynamic glass transition from an elastic to a viscous response. Moreover, the primary α relaxation in MGs exhibits a characteristic non-exponentiality (Yu et al., 2010b). Li et al. demonstrated that the microstructure features of MGs were thoroughly evaluated by performing statistical nanoindentation pop-in tests on MGs (Li et al., 2013). The structural heterogeneity of MGs was also revealed by mechanical spectroscopy and nanoindentation experiments (Tao et al., 2021). DMA is widely used to detect the atomic or molecular rearrangements associated with motions of "defects" in glassy solids (Khanna et al., 1985; Rotter and Ishida, 1992; Wang, 2019). The normalized storage modulus $\frac{E'}{E_u}$ and loss modulus $\frac{E''}{E_u}$ of the $Pd_{20}Pt_{20}Cu_{20}Ni_{20}P_{20}$ HE-MG at a frequency of 1 Hz are shown in Fig. 2 (a) as a function of temperature. The normalized storage and loss moduli remain almost constant below 450 K. Above this temperature, both slow β relaxation and primary α relaxation take place. The "shoulder" observed in the loss modulus from 450 to 520 K corresponds to the slow β relaxation. On further increase of temperature, the primary α relaxation, related to the dynamic glass transition phenomenon, appears at around 580 K. The intensity of the secondary relaxation on metallic glasses is quite different depending on their main constituent atom, as shown in Fig. 2 (b). La-based metallic glasses such as $La_{30}Ce_{30}Al_{15}Co_{25}$ show an evident slow β relaxation peak, while Pd-based such as $Pd_{42.5}Cu_{30}Ni_{7.5}P_{20}$ exhibit a shoulder and Zr- and Pt-based MG such as $Zr_{50}Cu_{40}Al_{10}$ and $Pt_{60}Ni_{15}P_{25}$ show only an excess wing. The $Pd_{20}Pt_{20}Cu_{20}Ni_{20}P_{20}$ HE-MG studied here shows an evident shoulder, similarly to $Pd_{42.5}Cu_{30}Ni_{7.5}P_{20}$ MG.

Mechanical relaxation processes show strongly driving frequency dependence. Fig. 2 (c) shows the temperature dependence of the normalized $\frac{E''}{E_u}$ at a heating rate of 3 K/min with various driving frequencies. The broad shoulder (β relaxation) around 500–560 K can be observed. The temperature of the β relaxation shifts towards higher temperature with increasing driving frequencies. The insert graph in Fig. 2 (c) exhibits the frequency dependence of the slow β relaxation, which was fitted to an Arrhenius law $f = f_\infty \exp\left(-\frac{E_\beta}{k_B T}\right)$ (Yu et al., 2012a). Here E_β is the activation energy of β relaxation, f_∞ is a pre-factor, and T is the temperature. A horizontal line was drawn in Fig. 2 (c) in order to determine the temperature of a given relaxation intensity, the details of this method can be found in (Yu et al., 2010a). Each intersection defines a point of frequency and temperature (f, T). Then these points were plotted into the Arrhenius map shown in the inset of Fig. 2 (c). The resulting activation energy from the Arrhenius fitting is $E_\beta = 191.31$ kJ/mol $= 1.98$ eV. The value $\frac{E_\beta}{k_B T_g} = 40$, is remarkably higher than the prediction of the empirical law $\frac{E_\beta}{k_B T_g} \approx 26$ for the activation energy of β relaxation in MGs (Ngai and Capaccioli, 2004; Sun et al., 2014b; Wang, 2019; Yu et al., 2012a, 2013). It appears that the β relaxation and α relaxation behaviors of MGs and HE-MGs are similar (Zhang et al., 2021b). Remarkably, $Pd_{20}Pt_{20}Cu_{20}Ni_{20}P_{20}$ HE-MG shows the highest activation energy E_β, suggesting that HE-MGs may have a higher energy barrier for the dynamic β relaxation.

According to literature, the microstructural origin of the slow β relaxation is linked to the structure heterogeneity and the motion of the atoms in soft regions (Huang et al., 2020; Wang et al., 2017; Wang, 2012; Yu et al., 2012a). From the viewpoint of structural dynamic heterogeneity (Tanaka et al., 2010; Wang et al., 2015; Ye et al., 2010), an external perturbation give rise to a relaxation process that probes the atomic mobility of MGs (Angel, 2000). Therefore, the dynamic mechanical relaxation spectra of MGs can shed light on the hidden dynamic structural properties and provide a way to understand the deformation, glass transition and diffusion behaviors of MGs (Ngai, 2011; Wang et al., 2015; Yu et al., 2012b).

Based on different theoretical models, β relaxation is associated to the "defects" of metallic glasses, i.e. excess free volume (Bletry et al., 2006), flow units (Wang, 2019), quasi-point defects (Perez, 1990) or interstitial defects (Khonik, 2015). The β relaxation in MGs can generate macroscopic tensile ductility (Yu et al., 2012b), enhance the diffusion of small atoms (Yu et al., 2012a), and trigger the activation of the shear-transformation-zones (STZ) (Liu et al., 2014) or flow units in MGs (Wang, 2019). To investigate the link between the structural heterogeneity and the slow β relaxation process, the microstructure of $Pd_{20}Pt_{20}Cu_{20}Ni_{20}P_{20}$ HE-MG was modified by quenching the Pd-based HE-MGs with different cooling rates. Samples were quenched at cooling rates of $\sim 10^3$ K/s (for bulk) and $\sim 10^5$ K/s (for ribbon). Fig. 2 (d) displays the effect of cooling rate on the slow β relaxation of $Pd_{20}Pt_{20}Cu_{20}Ni_{20}P_{20}$ in both bulk and ribbon samples. At low temperature, the normalized loss modulus $\frac{E''}{E''_{max}}$ of the ribbon sample is higher than that of bulk sample, and the value is nearly constant for both samples. With increasing temperature, the spectrum shows a β relaxation feature, which is remarkably more intense in the ribbon than in the bulk, similar results has been found in La-based MGs (Zhao et al., 2014). The intensity of the slow β relaxation is therefore strongly dependent on the glass state achieved during the quenching of HE-MGs. In fact, the

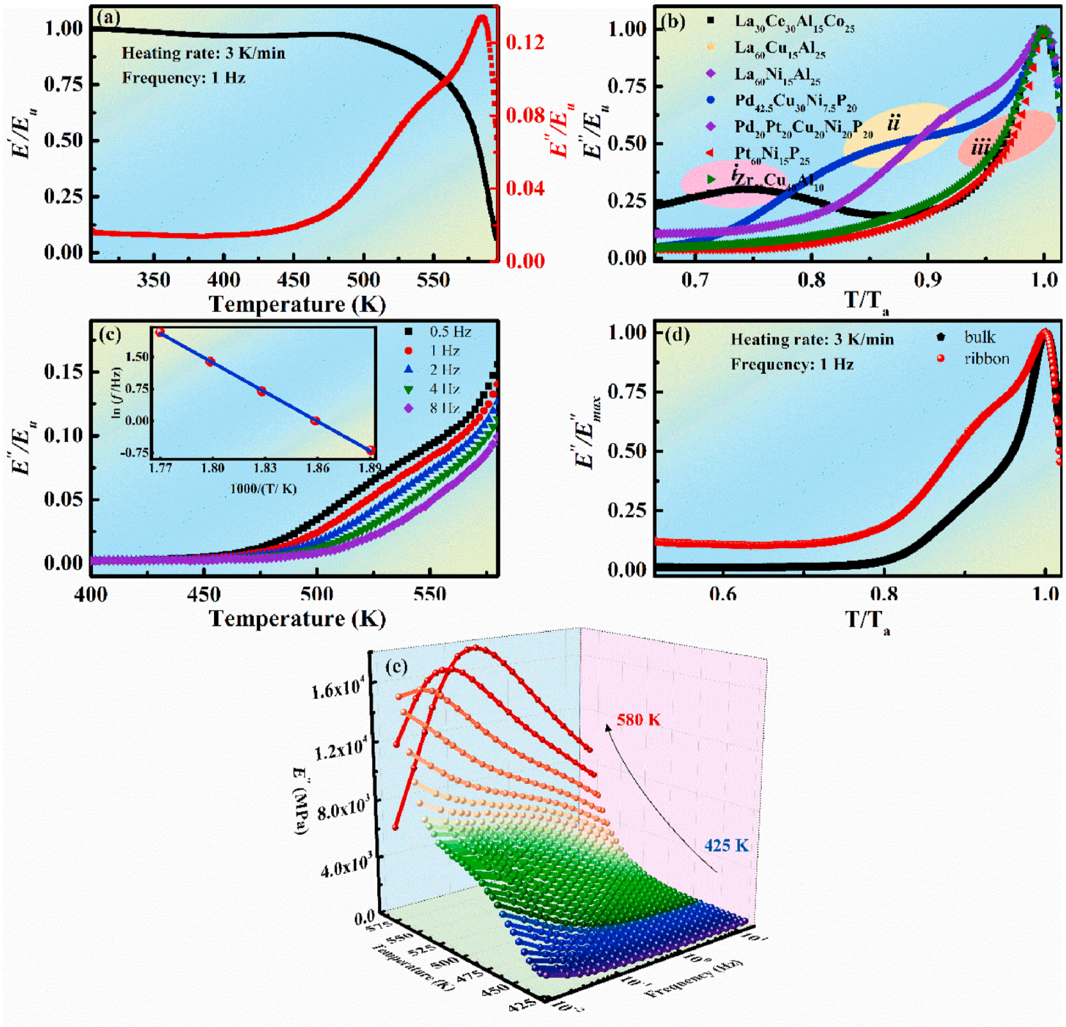

Fig. 2. Dynamic mechanical properties of the $Pd_{20}Pt_{20}Cu_{20}Ni_{20}P_{20}$ HE-MG. (a) Storage modulus $\frac{E'}{E_u}$ and loss modulus $\frac{E''}{E_u}$ of a ribbon sample as a function of temperature. The driving frequency is 1 Hz and the heating rate is 3 K/min E_u is taken as the value of the storage modulus at room temperature. (b) Normalized loss modulus $\frac{E''}{E_u}$ of $La_{30}Ce_{30}Al_{15}Co_{25}$, $Pd_{42.5}Cu_{30}Ni_{7.5}P_{20}$, $Pd_{20}Pt_{20}Cu_{20}Ni_{20}P_{20}$, $Pt_{60}Ni_{15}P_{25}$, and $Zr_{50}Cu_{40}Al_{10}$ ribbon metallic glasses as a function of the normalized temperature T/T_α. The driving frequency is 1 Hz, the heating rate is 3 K/min and T_α denotes the peak temperatures of α relaxation in the corresponding glass. (c) Normalized loss modulus $\frac{E''}{E_u}$ of $Pd_{20}Pt_{20}Cu_{20}Ni_{20}P_{20}$ bulk samples at a heating rate of 3 K/min and different driving frequencies ranging from 0.5 Hz to 8 Hz. The inset plot shows the logarithm of the frequency versus $\frac{1}{T}$. The solid line represents the Arrhenius fit. (d) Normalized loss modulus $\frac{E''}{E''_{max}}$ of $Pd_{20}Pt_{20}Cu_{20}Ni_{20}P_{20}$ in both bulk and ribbon samples. Heating rate is 3 K/min and driving frequency is 1 Hz. (e) Loss modulus E'' of $Pd_{20}Pt_{20}Cu_{20}Ni_{20}P_{20}$ as a function of frequency (ranging from 10^{-2} to 16 Hz) at various temperatures (425-430-435 … 580 K).

"shoulder" observed in the ribbon becomes almost an excess wing in the bulk. This phenomenon proves that higher cooling rates induce higher concentrations of the defects frozen in the HE-MG, as well as a more heterogeneous structure (Zhao et al., 2014). Although there is a weak link between the cooling rate and the position of the α relaxation, the curves also demonstrate a difference of the α relaxation peaks. The low-temperature wing of the α relaxation for the ribbon sample is wider than that of the bulk sample. Therefore, it is universal in MGs that the change of β relaxation and the low-temperature wing of α relaxation is due to the change of the structural heterogeneity and the alteration of the "defects" frozen in HE-MGs (Angel, 2000; Zhao et al., 2014).

In order to further understand the influence of the testing frequency on the dynamic mechanical processes of $Pd_{20}Pt_{20}Cu_{20}Ni_{20}P_{20}$ HE-MG, Fig. 2 (e) presents the frequency dependence of loss modulus E'' at various temperatures. The results show that at low temperature the loss modulus E'' increases by decreasing the frequency. The loss modulus shows a pronounced slow β relaxation shoulder by increasing the temperature. Eventually, a peak is observed around 560 K in the testing frequency window, which is associated with the primary α relaxation.

3.3. Stress relaxation

The mechanical relaxation curves of $Pd_{20}Pt_{20}Cu_{20}Ni_{20}P_{20}$ HE-MG under tensile stress at various temperatures from 385 to 575 K are shown in Fig. 3 (a). The time dependent relaxation curves can be well fitted by the phenomenological Kohlrausch-Williams-Watts (KWW) equation (Wang et al., 2014b; Williams and Watts, 1970; Zhao et al., 2015),

$$\sigma(t) = \sigma_0 \exp\left(-\frac{t}{\tau_c}\right)^{\beta_{KWW}} \tag{1}$$

where $\sigma(t)$ is the stress at time t, σ_0 is the initial stress, β_{KWW} is a stretched exponential parameter linked to dynamic heterogeneity and τ_c is the characteristic time of the relaxation mechanism (Lu et al., 2015; Wang et al., 2014b).

According to Fig. 3 (a), the stress σ_t decreases rapidly from the initial

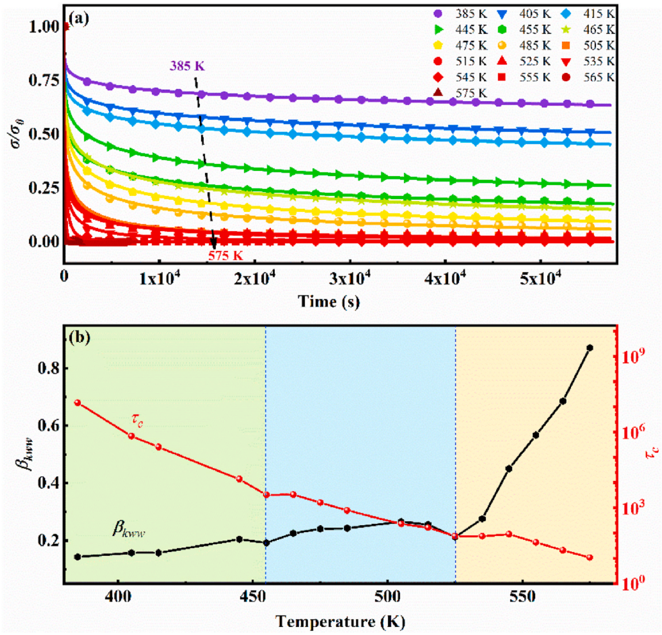

Fig. 3. Stress relaxation of $Pd_{20}Pt_{20}Cu_{20}Ni_{20}P_{20}$ HE-MG. (a) Stress relaxation spectra at various temperatures from 385 to 575 K ($T_g = 572$ K). The stresses σ_t were normalized by the corresponding initial stresses σ_0. The solid line is the result of the phenomenological KWW fittings. (b) The fitting parameters β_{KWW} and τ_c as a function of temperature.

stress σ_0, then declines slowly with time. Eventually, the stress tends to reach a minimum at the end of the experimental time window. As one can notice, the stress relaxation curves decay to zero at high temperatures, similar experimental results have been found in Zr-based MGs (Luo et al., 2017). During the stress relaxation process, the elastic strain gradually changes into the inelastic strain (Jiao et al., 2013a). The fitting parameters of the distribution coefficient β_{KWW} and the characteristic relaxation time τ_c at various temperatures during stress relaxation tests are shown in Fig. 3 (b). The characteristic stress relaxation time τ_c decreases by increasing temperature. The smaller the characteristic relaxation time τ_c, the faster the equilibrated state can be reached in the metallic glass system (Duan et al., 2020; Jiao et al., 2013a).

The parameter β_{KWW} reflects the width of the distribution of stress relaxation times. A larger β_{KWW} corresponds to smaller dynamic heterogeneity in metallic glasses (Ediger, 2000; Wang, 2019; Zhao et al., 2015). Similar experimental results have been reported in other typical MGs (Duan et al., 2020; Ediger, 2000; Harmon et al., 2007; Lu et al., 2014; Zhao et al., 2015). The parameter β_{KWW} increases from 0.12 to 0.87 with increasing temperature in $Pd_{20}Pt_{20}Cu_{20}Ni_{20}P_{20}$ HE-MG, indicating a decrease of the dynamic heterogeneity. However, the increase of parameter β_{KWW} is not continuous. The value of β_{KWW} increases slightly below 525 K, while increases substantially at higher temperatures. This phenomenon may be related to the stress relaxation mechanism in HE-MG. The transition temperature (~525 K) is very close to the onset of the primary relaxation (α relaxation), as can be seen in Fig. 2 (a), which reveals that the dynamic heterogeneity and structural relaxation are closely correlated with each other.

Stress relaxation in metallic alloys shows generally a logarithmic decline tendency (Chen et al., 2014; Kawamura et al., 1998; Wang et al., 2016; Yang et al., 2020). We define $n = \sigma_0 - \sigma_r$ as the intensity of the whole stress relaxation, where σ_0, and σ_r represent the initial stress and the residual stress, respectively. The parameter n gives the attenuation degree of stress relaxation in the $Pd_{20}Pt_{20}Cu_{20}Ni_{20}P_{20}$ HE-MG. The values of parameter n represent how fast the stochastic activation of the deformation units drives the corresponding stress relaxation processes, which can reflect the intrinsic nature of a glassy solid (i.e. structural heterogeneity and density of deformation units) (Lu et al., 2015; Pei et al., 2020). The n values of stress relaxation of $Pd_{20}Pt_{20}Cu_{20}Ni_{20}P_{20}$ HE-MG at various temperatures are displayed in Fig. 4. Fig. 4 shows that the intensity of stress relaxation increases almost linearly below 485 K, and then increases slower at higher temperature, and eventually it saturates above 525 K. It is proved that a higher value of n corresponds to a larger Poisson's ratio (Lu et al., 2015). Furthermore, the intensity of stress relaxation $\delta = \frac{\sigma_0 - \sigma_r}{\sigma_r}$ was proposed as a proper parameter to describe the features of the whole stress relaxation. It can be seen from Fig. 4 that the stress relaxation intensity δ increases slowly below 525 K, and rises rapidly above 525 K. The evolution of the parameter δ with temperature shows the same tendency than the KWW exponent β_{KWW}. Therefore, the noticeable change in behavior at 525 K may be correlated to the critical temperature of the relaxation time and relaxation intensity. It may be accompanied by a shift on the stress relaxation mechanism.

3.4. Mechanism-based linear relaxation modeling of stress relaxation

3.4.1. Linear relaxation model

The phenomenological KWW model has been widely used to describe the viscoelastic deformation (i.e. isothermal annealing, stress relaxation and creep deformation) of MGs (Qiao et al., 2019b; Sun and Wang, 2015; Wang, 2012; Williams and Watts, 1970). Typically, the evolution of relaxation events includes various relaxation characteristic times spanning many orders of magnitude, and a wide spectrum of activation barriers. Unfortunately, the KWW model fails to describe relaxation times at different time scale. To understand the activation process of the deformation units and the viscoelastic behavior of the HE-MG, a set of deformation units with different relaxation times τ_i ($i = 1{:}4$) scattered in the HE-MG and confined by the elastic matrix, as shown in Fig. 5 (a), will be used here as model. When stress is applied, the deformation units can be activated with several energy barriers (Argon and Kuo, 1980). Here we propose a generalized Maxwell linear relaxation model (see Fig. 5 (b)), which can be used to analyze the stress relaxation of glass solids. The linear relaxation model consists of a spring coupled in parallel to several spring-dashpot units. The spring-dashpot unit following the Newtonian law is usually regarded as an adequate description of the deformation units of MGs (Jiao et al., 2013b; Wang, 2012); the width of the distribution of deformation units with different characteristic times is related to the values of the Kohlrausch exponent β_{KWW}, while the springs obeying Hooke's law are a simplified description of the elastic matrix. According to the results of a model with more spring-dashpot units (see Fig. S1 and Fig. S2 in Appendix B), we judge that a linear relaxation model of 1 spring +4 spring-dashpot units is adequate to describe the hierarchical dynamics of the stress relaxation of

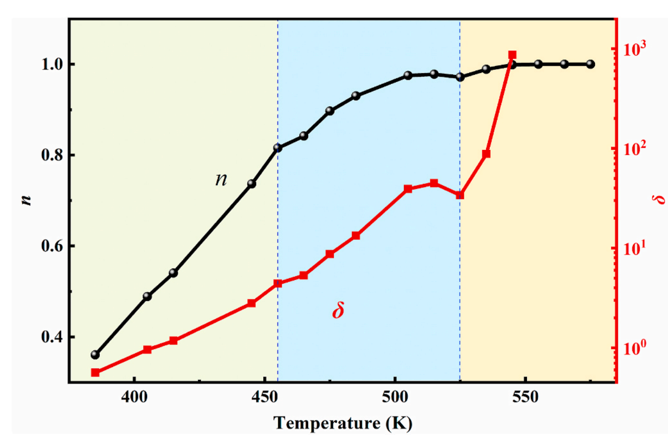

Fig. 4. Parameter n and the stress relaxation intensity δ of the stress relaxation model.

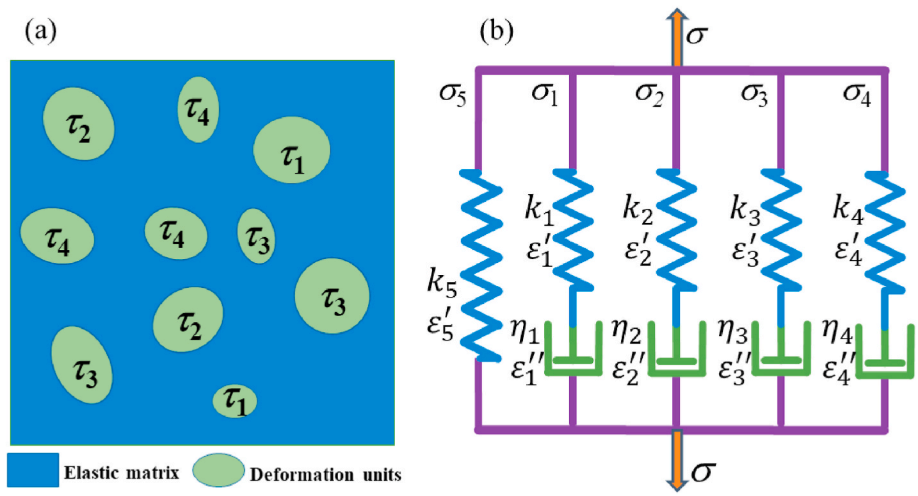

Fig. 5. (a) Schematic diagram of a HE-MG composed of deformation units embedded in an elastic matrix. (b) Schematic illustration of the corresponding linear relaxation model.

$Pd_{20}Pt_{20}Cu_{20}Ni_{20}P_{20}$ HE-MG.

As the derivation process of this linear relaxation model is very extensive, the detailed derivation is shown in Appendix A. The final linear relaxation equation is as follows

$$\sigma = A_1 \exp\left(-\frac{t}{\tau_1}\right) + A_2 \exp\left(-\frac{t}{\tau_2}\right) + A_3 \exp\left(-\frac{t}{\tau_3}\right) + A_4 \exp\left(-\frac{t}{\tau_4}\right) \quad (2)$$

where τ_i ($i = 1$, 2, 3 and 4) are the relaxation times, A_i ($i = 1$, 2, 3 and 4) are material-specific parameters representing the intensity of every relaxation time τ_i and $A_1 + A_2 + A_3 + A_4 = \sigma_0$. We will discuss the physical meaning of the corresponding parameters in the next section.

3.4.2. *Mechanical inhomogeneity and multi-relaxation process*

It is well documented that the phenomenological KWW model is suitable to describe a distribution of relaxation times with an average (or main) relaxation time. However, direct numerical spectrum analysis indicates that several relaxation times may coexist in MGs (Ju et al., 2011). The instantaneous relaxation events are likely to generate a multimodal distribution, with well-defined relaxation times which may be well described by the linear relaxation model solution given by Eq. (2). The orders of magnitude of these relaxation times may be different.

The fitted stress relaxation curves of the linear relaxation model at various temperatures are displayed in Fig. 6 (a) along with the experimental data. It can be noted that the stress relaxation behavior of the $Pd_{20}Pt_{20}Cu_{20}Ni_{20}P_{20}$ HE-MG is properly described by Eq. (2) in the studied temperature range. Fig. 6 (b) shows the results of the multimodal distribution of relaxation times of the linear relaxation model of stress relaxation (Eq. (2)). The radius of the symbol of the characteristic relaxation time is proportional to the corresponding intensity A_i ($i = 1$, 2, 3 and 4) in Eq. (2), which are also shown in Fig. 7. The characteristic times of the stress relaxation are distributed over several orders of magnitude, within the experimental time window. As expected, the characteristic times during the stress relaxation of $Pd_{20}Pt_{20}Cu_{20}Ni_{20}P_{20}$ HE-MG decrease with increasing testing temperature.

The characteristic time τ_1 in Fig. 6 (b) of the fastest relaxation event is ~100 s, and the intensity A_1 is not sensitive to temperature as shown in Fig. 7 (a). The remaining three characteristic times τ_i ($i = 2$, 3 and 4) in Fig. 6 (b) during the stress relaxation are several orders of magnitude larger than the characteristic time τ_1. As the stress relaxation process advances, the elastic strain of the spring elements in the linear relaxation model is slowly converted to inelastic strain of dashpot elements; similar results came up in other MGs (Bulatov and Argon, 1994; Jiao et al., 2013a). All the characteristic times τ_i ($i = 1$, 2, 3 and 4) in Fig. 6 (b) decay with increasing temperature in the whole range of temperatures

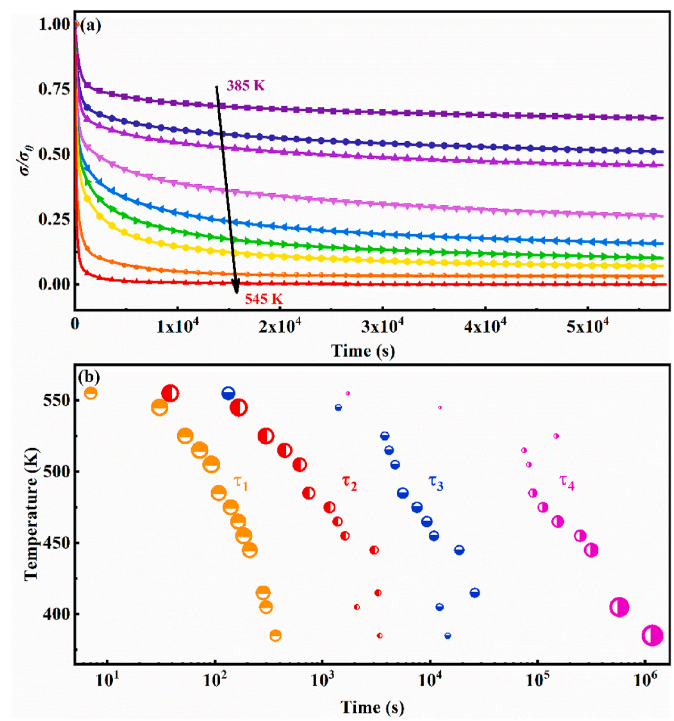

Fig. 6. (a) Comparison of experimental (symbols) and the linear relaxation model (solid lines) in stress relaxation at various temperatures. (b)The relaxation times τ_i ($i = 1$, 2, 3 and 4) fitted with Eq. (2). The size of the symbol is proportional to the corresponding intensity A_i ($i = 1$, 2, 3 and 4).

tested, which is associated with larger atomic mobility in MGs with increasing temperature (Duan et al., 2020; Khonik and Kobelev, 2019).

The linear relaxation model developed above can well fit the whole stress relaxation process within a wide range of temperature. The thermal effect is more obvious by increasing temperature. As a result, it takes less relaxation time to reach an equilibrium state. The stress relaxation behavior is dominated by all four relaxation times at low temperatures, while at high temperatures, the stress relaxation process is dominated by the two shorter relaxation times τ_1 and τ_2. It is interesting to note that the increase in β_{KWW} shown in Fig. 3 (b) above 525 K coincides with the total vanishing of the largest relaxation time τ_4, as expectable, which is accompanied by an increase of the intensity A_3 of τ_3. The 4-modal

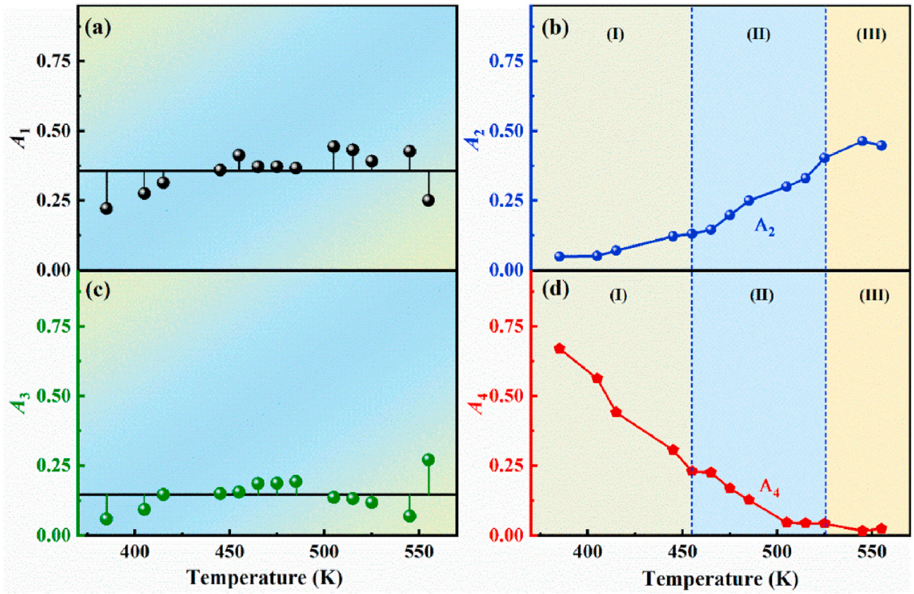

Fig. 7. Intensities A_i ($i = 1$, 2, 3 and 4) in Eq. (2).

distribution of relaxation times is dominated by 3-modes at 525 K. The heterogeneity of the glass is then decreased, as it is manifested by the sudden increase of the β_{KWW} exponent.

3.5. Activation energy spectra

There are significant differences in the structure of MGs due to structural heterogeneity. MGs contain loosely bonded regions or deformation units (Argon and Kuo, 1980; Ye et al., 2010). The width of the stretched exponential distribution of stress relaxation in MGs is also a clue indicating that the energy barrier of deformation units may be widely distributed.

The stress relaxation data and the activation energy spectrum model allow us to estimate the activation energy distribution and the evolution of the deformation units in MGs. The variation of the relaxation stress can be expressed by an integral equation (Gibbs et al., 1983),

$$\Delta\sigma(\mathrm{t}) = \int_0^{+\infty} p(E_a)\theta(E_a, T, t)dE_a \tag{9}$$

where $p(E_a)$ is the entire available property change caused by all the activation processes in the range of E_a to $E_a + dE_a$, and $\theta(E_a, T, t) = 1-\exp\left[-\nu_0 t \exp\left(\frac{E_a}{k_B T}\right)\right]$ is the characteristic annealing function (Gibbs et al., 1983). Here, ν_0 is the Debye frequency $\sim 10^{13}\ \mathrm{s}^{-1}$. The activation energy E_U of the deformation unit is critical and only those deformation units with $E_a < E_U$ contribute to the stress relaxation (Gibbs et al., 1983). In the step-like approximation,

$$p(E_a) = -\frac{1}{k_B T}\frac{d\sigma(t)}{d\ln(t)} \tag{10}$$

According to the Arrhenius equation,

$$E_a = k_B T \ln(\upsilon_0 t) \tag{11}$$

The apparent activation energy spectra with stress relaxation are shown in Fig. 8 (a). In order to compare the relative variation of activation energy spectra at different temperatures, $p(E_a)$ is normalized by the value at the maximum P_u. One can notice that the shape of the activation energy spectra of stress relaxation is close to a Gaussian distribution. By increasing the temperature, the trend of this distribution becomes more pronounced. The activation energy spectrum shifts towards higher activation energy with increasing temperature while the full width at half maximum (FWHM), shown in Fig. 8 (b), decreases. This indicates that more deformation units with higher energy barriers are activated during the stress relaxation at elevated temperature. It is interesting to note that some low temperature barriers, present at low temperatures, vanish at higher temperatures. These barriers, however, correspond to actual shear transformation zones which cannot vanish. Actually, the STZ with lower energies are annealed during the structural relaxation occurred during the heating process, and as a consequence their energies shift to higher values. This factor contributes to the reduction of the FWHM of the energy distribution at higher

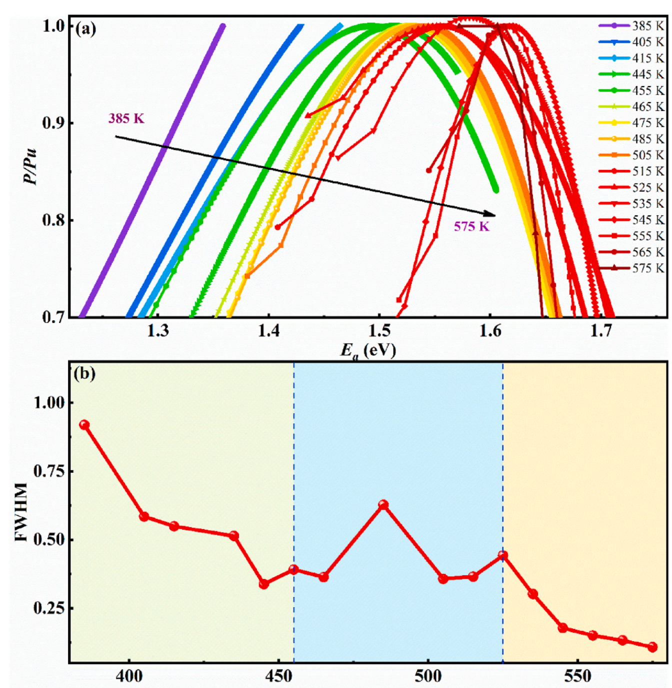

Fig. 8. (a) Temperature dependence of the normalized activation energy spectra for $Pd_{20}Pt_{20}Cu_{20}Ni_{20}P_{20}$ HE-MG at various temperatures, (b) The variation of FWHM of the activation energy spectra.

temperatures.

Due to the limited experimental time window of our experiments, only part of the $p(E_a)$ curve below 415 K is shown in the activation energy spectrum. The activation energy E_a of $Pd_{20}Pt_{20}Cu_{20}Ni_{20}P_{20}$ HE-MG is higher than that of Pd_{40} $Ni_{10}Cu_{30}P_{20}$ MG (Jiao et al., 2013b) and $La_{(60\text{-}x)}Ni_{15}Al_{25}Cu_x$ (x = 0, 2, 5 and 10) MG (Lu et al., 2016). This may indicate that the deformation units of $Pd_{20}Pt_{20}Cu_{20}Ni_{20}P_{20}$ HE-MG are more difficult to be activated than those of conventional MGs.

The changes of the deformation units (or soft regions) in the microstructure of the $Pd_{20}Pt_{20}Cu_{20}Ni_{20}P_{20}$ HE-MG can be associated to three processes, i.e., deformation unit stochastic activation process, deformation units proliferation process and deformation units penetration process. The FWHM of the activation energy spectrum decreases as temperature increases, which suggests that the distribution of deformation units is more homogeneous. A larger number of deformation units with different relaxation times τ_i ($i = 1$, 2, 3 and 4) with different activation energies participate in the stress relaxation process by increasing the temperature. When the temperature is below 455 K, the FWHM of activation energy spectrum is higher (as shown in Fig. 8 (b), which is in good accordance with the smaller value of the parameter β_{KWW} in Fig. 3 (b). It means that the microstructure of HE-MG is more heterogeneous, and only the deformation units with the smaller energy barriers are activated (Sun et al., 2014a; Wang, 2011; Zhao et al., 2015). The corresponding stress relaxation behavior presents an unobvious decay and the stress relaxation intensity δ in Fig. 4 (b) is very low. When the temperature ranges between 455 and 525 K, the annealing process during the heating protocol increases the activation energy of the softest deformation units, inducing a decrease of the FWHM. But due to the higher temperature, deformation units with higher energy barriers are activated. The density of deformation units raises, which corresponds to the proliferation process of deformation units. This results in a narrower distribution of the activation energy spectrum, which is associated with the decrease of dynamical heterogeneity of the $Pd_{20}Pt_{20}Cu_{20}Ni_{20}P_{20}$ HE-MG and reflected in a moderate increase in the value of β_{KWW} (Duan et al., 2020; Sun et al., 2014a; Wang et al., 2014b). Therefore, the stress relaxation intensity δ increases. When the temperature is further increased (above 525 K), the stress relaxation mechanism is dominated by the thermal excitation as shown in Fig. 6 (b). The parameter β_{KWW} increases rapidly, the microstructure of $Pd_{20}Pt_{20}Cu_{20}Ni_{20}P_{20}$ HE-MG is largely more homogenous. The activation energy spectrum shifts towards higher values and its FWHM decreases substantially. The fraction of the deformation units expand rapidly corresponding to the penetration process (Sun et al., 2014a; Wang et al., 2014b). The process swings from elastic deformation to inelastic deformation in $Pd_{20}Pt_{20}Cu_{20}Ni_{20}P_{20}$ HE-MG. The results further confirmed that the statistical distribution of deformation units is closely related to the heterogeneity of $Pd_{20}Pt_{20}Cu_{20}Ni_{20}P_{20}$ HE-MG.

4. Conclusion

In summary, the viscoelastic deformation of a $Pd_{20}Pt_{20}Cu_{20}Ni_{20}P_{20}$ high-entropy metallic glass was studied by mechanical spectroscopy and stress relaxation. Physical insights into the microstructure-induced dynamical heterogeneity, and their decoupling, were obtained from combined methodologies of experiments, theory and modeling. The dynamic mechanical relaxation process (i.e. β relaxation and α relaxation) was investigated by mechanical spectroscopy over a wide range of temperature and frequency. It is found that the stress relaxation in this high-entropy glass can be well described by the Kohlrausch-Williams-Watts equation. The determined stretching exponents indicate a trend of reduced dynamic heterogeneity with increasing temperature, which echoes also in the decrease of the full width at half maximum of the energy barrier spectra. A linear relaxation model was developed to analyze the stress relaxation process in the studied temperature range. The results of activation energy spectra at various temperatures revealed the interplay between the increase of the population of deformation units and the elastic-to-plastic transition in the relaxation process as temperature approaches the glass transition of the HE-BMG.

Credit author contribution statement

J.Y. Duan: Conceptualization, Data curation, Formal analysis, Investigation, Methodology, Writing – original draft, Writing – review & editing. **J.C. Qiao**: Conceptualization, Formal analysis, Project administration, Resources, Funding acquisition, Methodology, Supervision, Writing – original draft, Writing – review & editing. **T. Wada**: Investigation, Methodology, Writing – review & editing. **H. Kato**: Investigation, Methodology, Writing – review & editing. **E. Pineda**: Formal analysis, Project administration, Resources, Funding acquisition, Methodology, Supervision, Writing – original draft, Writing – review & editing. **D. Crespo**: Formal analysis, Project administration, Resources, Funding acquisition, Methodology, Supervision, Writing – original draft, Writing – review & editing. **Y.J. Wang**: Conceptualization, Formal analysis, Methodology, Software, Funding acquisition, Writing – original draft, Writing – review & editing.

Declaration of competing interest

Regarding to this paper, which entitled as "Stress relaxation in high-entropy $Pd_{20}Pt_{20}Cu_{20}Ni_{20}P_{20}$ metallic glass considering structural heterogeneity: Experiments, modeling and theory" co-authored by Y.J. Duan, J.C. Qiao, T. Wada, H. Kato, E. Pineda, D. Crespo & Y.J. Wang, which we wish to be considered for publication in ***Mechanics of Materials.*** All the co-authors have no conflicts of interest to declare.

Acknowledgment

This work is supported by the NSFC (Grant No. 51971178) and the Natural Science Basic Research Plan for Distinguished Young Scholars in Shaanxi Province (Grant No. 2021JC-12). E. Pineda and D. Crespo acknowledge financial support from MICINN (grant FIS2017-82625-P) and Generalitat de Catalunya (grant 2017SGR0042). The investigation of Y. J. Duan sponsored by Innovation Foundation for Doctor Dissertation of Northwestern Polytechnical University (No. CX202031) and China Scholarship Council (CSC) under Grant 202006290092. Y.J. Wang acknowledge the NSFC (Grants No. 12072344) and the Youth Innovation Promotion Association of Chinese Academy of Sciences (Grant No. 2017025).

Appendix A. Supplementary data

Supplementary data to this article can be found online at https://doi.org/10.1016/j.mechmat.2021.103959.

References

Angel, C.A., 2000. Relaxation in glassforming liquids and amorphous solids. J. Appl. Phys. 88, 3113–3157.
Argon, A.S., Kuo, H.Y., 1980. Free energy spectra for inelastic deformation of five metallic glass alloys. J. Non-Cryst. Solids 37, 241–266.
Bharathula, A., Flores, K.M., 2011. Variability in the yield strength of a metallic glass at micron and submicron length scales. Acta Mater. 59, 7199–7205.
Bletry, M., Guyot, P., Blandin, J.-J., Soubeyroux, J.-L., 2006. Free volume model: high-temperature deformation of a Zr-based bulk metallic glass. Acta Mater. 54, 1257–1263.
Bobrov, O., Csach, K., Khonik, S., Kitagawa, K., Lyakhov, S., Yazvitsky, M.Y., Khonik, V., 2007. The recovery of structural relaxation-induced viscoelastic creep strain in bulk and ribbon $Pd_{40}Cu_{30}Ni_{10}P_{20}$ glass. Scripta Mater. 56, 29–32.
Bulatov, V.V., Argon, A.S., 1994. A stochastic model for continuum elasto-plastic behavior. II. A study of the glass transition and structural relaxation. Modell. Simul. Mater. Sci. Eng. Anal. 2, 185–202.
Chen, J.F., Jiang, J.T., Zhen, L., Shao, W.Z., 2014. Stress relaxation behavior of an Al–Zn–Mg–Cu alloy in simulated age-forming process. J. Mater. Process. Technol. 214, 775–783.
Cheng, Y.T., Johnson, W.L., 1987. Disordered materials: a survey of amorphous solids. Science 235, 997–1002.

Cheng, Y.Q., Ma, E., 2011. Atomic-level structure and structure-property relationship in metallic glasses. Prog. Mater. Sci. 56, 379–473.

Cunliffe, A., Plummer, J., Figueroa, I., Todd, I., 2012. Glass formation in a high entropy alloy system by design. Intermetallics 23, 204–207.

Duan, Y.J., Yang, D.S., Qiao, J.C., Crespo, D., Pelletier, J.M., Li, L., Gao, K., Zhang, T., 2020. Relaxation of internal friction and shear viscosity in $Zr_{57}Nb_5Al_{10}Cu_{15.4}Ni_{12.6}$ metallic glass. Intermetallics 124, 106846.

Duine, P.A., Sietsma, J., Van, d.B.A., 1993. Atomic transport in amorphous $Pd_{40}Ni_{40}P_{20}$ near the glass-transition temperature: Au diffusivity and viscosity. Phys. Rev. B 48, 6957–6965.

Ediger, M.D., 2000. Spatially heterogeneous dynamics in supercooled liquids. Annu. Rev. Phys. Chem. 51, 99.

Flores, K.M., Sherer, E., Bharathula, A., Chen, H., Jean, Y.C., 2007. Sub-nanometer open volume regions in a bulk metallic glass investigated by positron annihilation. Acta Mater. 55, 3403–3411.

Fornell, J., Concustell, A., Surinach, S., Li, W.H., Cuadrado, N., Gebert, A., Baro, M.D., Sort, J., 2009. Yielding and intrinsic plasticity of Ti–Zr–Ni–Cu–Be bulk metallic glass. Int. J. Plast. 25, 1540–1559.

Fujita, T., Konno, K., Zhang, W., Kumar, V., Matsuura, M., Inoue, A., Sakurai, T., Chen, M.W., 2009. Atomic-scale heterogeneity of a multicomponent bulk metallic glass with excellent glass forming ability. Phys. Rev. Lett. 103, 075502.

García, R., Magerle, R., Perez, R., 2007. Nanoscale compositional mapping with gentle forces. Nat. Mater. 6, 405–411.

George, E.P., Raabe, D., Ritchie, R.O., 2019. High-entropy alloys. Nat. Rev. Mater. 4, 515–534.

Gibbs, M., Evetts, J., Leake, J., 1983. Activation energy spectra and relaxation in amorphous materials. J. Mater. Sci. 18, 278–288.

Glasscott, M.W., Pendergast, A.D., Goines, S., Bishop, A.R., Hoang, A.T., Renault, C., Dick, J.E., 2019. Electrosynthesis of high-entropy metallic glass nanoparticles for designer, multi-functional electrocatalysis. Nat. Commun. 10, 1–8.

Gleiter, H., 2016. Nanoglasses: a new kind of noncrystalline material and the way to an age of new technologies? Small 12, 2225–2233.

Goncharova, E., Konchakov, R., Makarov, A., Kobelev, N., Khonik, V., 2017. Identification of interstitial-like defects in a computer model of glassy aluminum. J. Phys. Condens. Mat. 29, 305701.

Greer, L.A., 1993. Confusion by design. Nature 366, 303–304.

Harmon, J.S., Demetriou, M.D., Johnson, W.L., Samwer, K., 2007. Anelastic to plastic transition in metallic glass-forming liquids. Phys. Rev. Lett. 99, 135502.

Herrero-Gómez, C., Samwer, K., 2016. Stress and temperature dependence of the avalanche dynamics during creep deformation of metallic glasses. Sci. Rep. 6, 1–6.

Highmore, R.J., Greer, A.L., 1989. Eutectics and the formation of amorphous alloys. Nature 339, 363–365.

Hirata, A., Guan, P., Fujita, T., Hirotsu, Y., Inoue, A., Yavari, A.R., Sakurai, T., Chen, M., 2011. Direct observation of local atomic order in a metallic glass. Nat. Mater. 10, 28–33.

Hu, Y.C., Guan, P.F., Li, M.Z., Liu, C.T., Yang, Y., Bai, H.Y., Wang, W.H., 2016. Unveiling atomic-scale features of inherent heterogeneity in metallic glass by molecular dynamics simulations. Phys. Rev. B 93, 214202.

Huang, B., Yuan, C., Wang, Z., Tong, Y., Wang, Q., Yi, J., Wang, G., He, Q., Shek, C., Yang, Y., 2020. Influence of short-to medium-range electronic and atomic structure on secondary relaxations in metallic glasses. Acta Mater. 196, 88–100.

Hufnagel, T.C., Schuh, C.A., Falk, M.L., 2016. Deformation of metallic glasses: recent developments in theory, simulations, and experiments. Acta Mater. 109, 375–393.

Ichitsubo, T., Matsubara, E., Yamamoto, T., Chen, H.S., Nishiyama, N., Saida, J., Anazawa, K., 2005. Microstructure of fragile metallic glasses inferred from ultrasound-accelerated crystallization in Pd-based metallic glasses. Phys. Rev. Lett. 95, 245501.

Inoue, A., Takeuchi, A., 2011. Recent development and application products of bulk glassy alloys. Acta Mater. 59, 2243–2267.

Jeong, H.T., Kim, J.H., Kim, W.T., Kim, D.H., 2004. The mechanical relaxations of a $Mm_{55}Al_{25}Ni_{10}Cu_{10}$ amorphous alloy studied by dynamic mechanical analysis. Mater. Sci. Eng. A 385, 182–186.

Jiao, W., Sun, B.A., Wen, P., Bai, H.Y., Kong, Q.P., 2013a. Crossover from stochastic activation to cooperative motions of shear transformation zones in metallic glasses. Appl. Phys. Lett. 103, 081904.

Jiao, W., Wen, P., Peng, H., Bai, H., Sun, B., Wang, W., 2013b. Evolution of structural and dynamic heterogeneities and activation energy distribution of deformation units in metallic glass. Appl. Phys. Lett. 102, 101903.

Johnson, W.L., 1999. Bulk glass-forming metallic alloys: science and technology. MRSBu 24, 42–56.

Ju, J.D., Atzmon, M., 2014. A comprehensive atomistic analysis of the experimental dynamic-mechanical response of a metallic glass. Acta Mater. 74, 183–188.

Ju, J., Jang, D., Nwankpa, A., Atzmon, M., 2011. An atomically quantized hierarchy of shear transformation zones in a metallic glass. J. Appl. Phys. 109, 053522.

Kato, H., Inoue, A., Chen, H.S., 2006. On structural relaxation and viscous work heating during non-Newtonian viscous flow in a ZrAlNiCu bulk metallic glass. Acta Mater. 54, 891–898.

Kawamura, Y., Shibata, T., Inoue, A., 1998. Changes in stress relaxation due to yielding in $Zr_{65}Al_{10}Ni_{10}Cu_{15}$ metallic glass. Jpn. J. Appl. Phys. 37, L666.

Ketov, S.V., Sun, Y.H., Nachum, S., Lu, Z., Checchi, A., Beraldin, A.R., Bai, H.Y., Wang, W.H., Louzguine-Luzgin, D.V., Carpenter, M.A., 2015. Rejuvenation of metallic glasses by non-affine thermal strain. Nature 524, 200–203.

Khanna, Y.P., Turi, E.A., Taylor, T.J., Vickroy, V.V., Abbott, R.F., 1985. Dynamic mechanical relaxations in polyethylene. Macromolecules 18, 1302–1309.

Khonik, V.A., 2015. Understanding of the structural relaxation of metallic glasses within the framework of the Interstitialcy theory. Metals 5, 504–529.

Khonik, V., Kobelev, N., 2019. Metallic glasses: a new approach to the understanding of the defect structure and physical properties. Metals 9, 605.

Kim, K., Das, J., Baier, F., Tang, M., Wang, W., Eckert, J.J.A.p.l., 2006. Heterogeneity of a $Cu_{47.5}Zr_{47.5}Al_5$ bulk metallic glass. Appl. Phys. Lett. 88, 051911.

Kim, D.H., Kim, W., Park, E., Mattern, N., Eckert, J., 2013. Phase separation in metallic glasses. Prog. Mater. Sci. 58, 1103–1172.

Kim, J., Oh, H.S., Kim, J., Ryu, C.W., Lee, G.W., Chang, H.J., Park, E.S., 2018. Utilization of high entropy alloy characteristics in Er-Gd-Y-Al-Co high entropy bulk metallic glass. Acta Mater. 155, 350–361.

Komazaki, S.-i., Kato, T., Kohno, Y., Tanigawa, H., 2009. Creep property measurements of welded joint of reduced-activation ferritic steel by the small-punch creep test. Mater. Sci. Eng. A 510, 229–233.

Krisponeit, J.O., Pitikaris, S., Avila, K.E., Küchemann, S., Krüger, A., Samwer, K., 2014. Crossover from random three-dimensional avalanches to correlated nano shear bands in metallic glasses. Nat. Commun. 5, 1–5.

Launey, M.E., Hofmann, D.C., Johnson, W.L., Ritchie, R.O., 2009. Solution to the problem of the poor cyclic fatigue resistance of bulk metallic glasses. Proc. Natl. Acad. Sci. U.S.A. 106, 4986–4991.

Lei, T., DaCosta, L.R., Liu, M., Shen, J., Sun, Y., Wang, W., Atzmon, M., 2020. Composition dependence of metallic glass plasticity and its prediction from anelastic relaxation–a shear transformation zone analysis. Acta Mater. 195, 81–86.

Li, W., Bei, H., Tong, Y., Dmowski, W., Gao, Y., 2013. Structural heterogeneity induced plasticity in bulk metallic glasses: from well-relaxed fragile glass to metal-like behavior. Appl. Phys. Lett. 103, 171910.

Li, C., Li, X., Zhao, Z., Zhu, F., Zhao, Y., 2019. Effect of peak loads and cooling rates on creep behavior of Zr-based bulk metallic glass. J. Non-Cryst. Solids 522, 119596.

Liu, Y.H., Fujita, T., Aji, D.P.B., Matsuura, M., Chen, M.W., 2014. Structural origins of Johari-Goldstein relaxation in a metallic glass. Nat. Commun. 5, 3238.

Lu, Z., Jiao, W., Wang, W.H., Bai, H.Y., 2014. Flow unit perspective on room temperature homogeneous plastic deformation in metallic glasses. Phys. Rev. Lett. 113, 045501.

Lu, Z., Wang, W.H., Bai, H.Y., 2015. Classification of metallic glasses based on structural and dynamical heterogeneities by stress relaxation. Sci. China. Mater. 58, 98–105.

Lu, Z., Shang, B.S., Sun, Y.T., Zhu, Z.G., Guan, P.F., Wang, W.H., Bai, H.Y., 2016. Revealing β-relaxation mechanism based on energy distribution of flow units in metallic glass. J. Chem. Phys. 144, 144501.

Luo, P., Wen, P., Bai, H.Y., Ruta, B., Wang, W.H., 2017. Relaxation decoupling in metallic glasses at low temperatures. Phys. Rev. Lett. 118, 225901.

Masumoto, T., Hashimoto, K., 1978. Chemical properties of amorphous metals. Annu. Rev. Mater. Res. 8, 215–233.

Miracle, D.B., Senkov, O.N., 2017. A critical review of high entropy alloys and related concepts. AcMat 122, 448–511.

Ngai, K.L., 2011. Relaxation and Diffusion in Complex Systems. Springer, New York.

Ngai, K., Capaccioli, S., 2004. Relation between the activation energy of the Johari-Goldstein β relaxation and T g of glass formers. Phys. Rev. E 69, 031501.

Ngai, K.L., Li-Min, W., Riping, L., Wang, W.H., 2014. Microscopic dynamics perspective on the relationship between Poisson's ratio and ductility of metallic glasses. J. Chem. Phys. 140, 044511.

Pei, C., Zhao, R., Fang, Y., Wu, S., Cui, Z., Sun, B., Lan, S., Luo, P., Wang, W., Feng, T., 2020. The structural and dynamic heterogeneities of Ni-P nanoglass characterized by stress-relaxation. J. Alloy Comd. 836, 155506.

Perez, J., 1990. Quasi-punctual defects in vitreous solids and liquid-glass transition. SSIon 39, 69–79.

Qiao, J.C., Wang, Y.J., Pelletier, J.M., Keer, L.M., Fine, M.E., Yao, Y., 2015. Characteristics of stress relaxation kinetics of $La_{60}Ni_{15}Al_{25}$ bulk metallic glass. Acta Mater. 98, 43–50.

Qiao, J.C., Wang, Y.J., Zhao, L.Z., Dai, L.H., Crespo, D., Pelletier, J.M., Keer, L.M., Yao, Y., 2016. Transition from stress-driven to thermally activated stress relaxation in metallic glasses. Phys. Rev. B 94, 104203.

Qiao, J.C., Liu, X.D., Wang, Q., Liu, C.T., Lu, J., Yang, Y., 2018. Fast secondary relaxation and plasticity initiation in metallic glasses. Natl. Sci. Rev. 5, 616–618.

Qiao, J.C., Pelletier, J.M., Yao, Y., 2019a. Creep in bulk metallic glasses. Transition from linear to non linear regime. Mater. Sci. Eng. A 743, 185–189.

Qiao, J.C., Wang, Q., Pelletier, J.M., Kato, H., Casalini, R., Crespo, D., Pineda, E., Yao, Y., Yang, Y., 2019b. Structural heterogeneities and mechanical behavior of amorphous alloys. Prog. Mater. Sci. 104, 250–329.

Rotter, G., Ishida, H., 1992. Dynamic mechanical analysis of the glass transition: curve resolving applied to polymers. Macromolecules 25, 2170–2176.

Ruitenberg, G., De Hey, P., Sommer, F., Sietsma, J., 1997. Pressure-induced structural relaxation in amorphous $Pd_{40}Ni_{40}P_{20}$: the Formation volume for diffusion defects. Phys. Rev. Lett. 79, 4830–4833.

Schroers, J., Johnson, W.L., 2005. Ductile bulk metallic glass. Phys. Rev. Lett. 93, 255506.

Schuh, C.A., Hufnagel, T.C., Ramamurty, U., 2007. Mechanical behavior of amorphous alloys. Acta Mater. 55, 4067–4109.

Sha, Z.-D., Branicio, P.S., Lee, H.P., Tay, T.E., 2017. Strong and ductile nanolaminate composites combining metallic glasses and nanoglasses. Int. J. Plast. 90, 231–241.

Sheng, H.W., Luo, W.K., Alamgir, F.M., Bai, J.M., Ma, E., 2006. Atomic packing and short-to-medium-range order in metallic glasses. Nature 439, 419–425.

Shu, F.Y., Wu, L., Zhao, H.Y., Sui, S.H., Zhou, L., Zhang, J., He, W.X., He, P., Xu, B.S., 2017. Microstructure and high-temperature wear mechanism of laser cladded CoCrBFeNiSi high-entropy alloy amorphous coating. Mater. Lett. 211, 235–238.

Spaepen, F., 1987. The art and science of microstructural control. Science 235, 1010–1014.

Sun, B.A., Wang, W.H., 2015. The fracture of bulk metallic glasses. Prog. Mater. Sci. 74, 211–307.

Sun, B., Liu, Z., Yang, Y., Liu, C., 2014a. Delayed shear banding and evolution of local plastic flow in a metallic glass. Appl. Phys. Lett. 105, 091904.

Sun, Q., Zhou, C., Yue, Y., Hu, L., 2014b. A direct link between the fragile-to-strong transition and relaxation in supercooled liquids. J. Phys. Chem. Lett. 5, 1170–1174.

Takeuchi, A., Chen, N., Wada, T., Yokoyama, Y., Kato, H., Inoue, A., Yeh, J.W., 2011. $Pd_{20}Pt_{20}Cu_{20}Ni_{20}P_{20}$ high-entropy alloy as a bulk metallic glass in the centimeter. Intermetallics 19, 1546–1554.

Tanaka, H., 2012. Bond orientational order in liquids: towards a unified description of water-like anomalies, liquid-liquid transition, glass transition, and crystallization. EPJE 35, 113.

Tanaka, H., Kawasaki, T., Shintani, H., Watanabe, K., 2010. Critical-like behaviour of glass-forming liquids. Nat. Mater. 9, 324–331.

Tao, K., Qiao, J.C., He, Q.F., Song, K.K., Yang, Y., 2021. Revealing the Structural Heterogeneity of Metallic Glass: Mechanical Spectroscopy and Nanoindentation Experiments. Inter. J. Mech. Sci. 201, 106469.

Tsai, P., Kranjc, K., Flores, K.M., 2017. Hierarchical heterogeneity and an elastic microstructure observed in a metallic glass alloy. Acta Mater. 139, 11–20.

Vempati, U.K., Valavala, P.K., Falk, M.L., Almer, J., Hufnagel, T.C., 2012. Length-scale dependence of elastic strain from scattering measurements in metallic glasses. Phys. Rev. B 85, 214201.

Wang, W.H., 2011. Correlation between relaxations and plastic deformation, and elastic model of flow in metallic glasses and glass-forming liquids. J. Appl. Phys. 110, 053521.

Wang, W.H., 2012. The elastic properties, elastic models and elastic perspectives of metallic glasses. Prog. Mater. Sci. 57, 487–656.

Wang, W.H., 2014. High-entropy metallic glasses. J. Occup. Med. 66, 2067–2077.

Wang, W.H., 2019. Dynamic relaxations and relaxation-property relationships in metallic glasses. Prog. Mater. Sci. 106, 100561.

Wang, Q., Yang, Y., Jiang, H., Liu, C.T., Ruan, H.H., Lu, J., 2014a. Superior tensile ductility in bulk metallic glass with gradient amorphous structure. Sci. Rep. 4, 4757.

Wang, Z., Sun, B., Bai, H., Wang, W., 2014b. Evolution of hidden localized flow during glass-to-liquid transition in metallic glass. Nat. Commun. 5, 5823.

Wang, Q., Zhang, S.T., Yang, Y., Dong, Y.D., Liu, C.T., Lu, J., 2015. Unusual fast secondary relaxation in metallic glass. Nat. Commun. 6, 7876.

Wang, Y., Dong, J., Zhang, M., Yao, Z., 2016. Stress relaxation behavior and mechanism of AEREX350 and Waspaloy superalloys. Mater. Sci. Eng. A 678, 10–22.

Wang, Q., Liu, J., Ye, Y., Liu, T., Wang, S., Liu, C., Lu, J., Yang, Y., 2017. Universal secondary relaxation and unusual brittle-to-ductile transition in metallic glasses. Mater. Today 20, 293–300.

Wang, G., Pan, D., Shi, X., Marko, H., Cao, W., Huang, Y., 2018a. Tensile creep characterization and prediction of Zr-based metallic glass at high temperatures. Metals 8, 457.

Wang, X., Dai, W., Zhang, M., Gong, P., Li, N., 2018b. Thermoplastic micro-formability of TiZrHfNiCuBe high entropy metallic glass. J. Mater. Sci. Technol. 34, 2006–2013.

Williams, G., Watts, D.C., 1970. Non-symmetrical dielectric relaxation behaviour arising from a simple empirical decay function. Trans. Faraday Soc. 66, 80–85.

Xu, Y., Shi, B., 2018. Effects of strain and strain rate on the evolution of shear bands for room temperature rolled $Pd_{40}Ni_{40}P_{20}$ bulk metallic glass. J. Non-Cryst. Solids 485, 74–81.

Yang, M., Liu, X.J., Ruan, H.H., Wu, Y., Wang, H., Lu, Z.P., 2016. High thermal stability and sluggish crystallization kinetics of high-entropy bulk metallic glasses. J. Appl. Phys. 119, 245112.

Yang, Y., Zhan, L., Liu, C., Wang, X., Wang, Q., Tang, Z., Li, G., Huang, M., Hu, Z., 2020. Stress-relaxation ageing behavior and microstructural evolution under varying initial stresses in an Al–Cu alloy: experiments and modeling. Int. J. Plast. 127, 102646.

Ye, J.C., Lu, J., Liu, C.T., Wang, Q., Yang, Y., 2010. Atomistic free-volume zones and inelastic deformation of metallic glasses. Nat. Mater. 9, 619–623.

Yu, H., Wang, W., Bai, H., Wu, Y., Chen, M., 2010a. Relating activation of shear transformation zones to β relaxations in metallic glasses. Phys. Rev. B 81, 220201.

Yu, H., Wang, W., Bai, H., Wu, Y., Chen, M., 2010b. Relating activation of shear transformation zones to β relaxations in metallic glasses. PhRvB 81, 220201.

Yu, H.B., Samwer, K., Wu, Y., Wang, W.H., 2012a. Correlation between β relaxation and self-diffusion of the smallest constituting atoms in metallic glasses. Phys. Rev. Lett. 109, 095508.

Yu, H.B., Shen, X., Wang, Z., Gu, L., Wang, W.H., Bai, H.Y., 2012b. Tensile plasticity in metallic glasses with pronounced β relaxations. Phys. Rev. Lett. 108, 015504.

Yu, H.B., Wang, W.H., Samwer, K., 2013. The β relaxation in metallic glasses: an overview. Mater. Today 16, 183–191.

Zhang, Y., Qiao, J.W., Kliaw, P., 2016. A brief review of high entropy alloys and serration behavior and flow units. J. Iron Steel Res. Int. 23, 2–6.

Zhang, M., Chen, Y., He, R., Guo, S., Ma, J., Dai, L., 2019. Probing the role of Johari–Goldstein relaxation in the plasticity of metallic glasses. Mater. Res. Lett. 7, 383–391.

Zhang, L.T., Duan, Y.J., Daniel, C., Eloi, P., Yunjiang, W., Pelletier, J.M., Jichao, Q., 2021a. Dynamic mechanical relaxation and thermal creep of high-entropy $La_{30}Ce_{30}Ni_{10}Al_{20}Co_{10}$ bulk metallic glass. Sci. China Phys. Mech. Astron. https://doi.org/10.1007/s11433-021-1722-y.

Zhang, L.T., Duan, Y.J., Wada, T., Kato, H., Pelletier, J.M., Crespo, D., Pineda, E., Qiao, J. C., 2021b. Dynamic mechanical relaxation behavior of $Zr_{35}Hf_{17.5}Ti_{5.5}Al_{12.5}Co_{7.5}Ni_{12}Cu_{10}$ high entropy bulk metallic glass. J. Mater. Sci. Technol. 83, 248–255.

Zhao, L.Z., Wang, W.H., Bai, H.Y., 2014. Modulation of β-relaxation by modifying structural configurations in metallic glasses. J. Non-Cryst. Solids 405, 207–210.

Zhao, L.Z., Li, Y.Z., Xue, R.J., Wang, W.H., Bai, H.Y., 2015. Evolution of structural and dynamic heterogeneities during elastic to plastic transition in metallic glass. J. Appl. Phys. 118, 154904.

Zhu, F., Nguyen, H.K., Song, S.X., Aji, D.P.B., Hirata, A., Wang, H., Nakajima, K., Chen, M.W., 2016. Intrinsic correlation between β-relaxation and spatial heterogeneity in a metallic glass. Nat. Commun. 7, 11516.

Zhu, F., Hirata, A., Liu, P., Song, S., Tian, Y., Han, J., Fujita, T., Chen, M., 2017. Correlation between local structure order and spatial heterogeneity in a metallic glass. Phys. Rev. Lett. 119, 215501.